Monitoring large oil slick dynamics with moderate resolution multispectral satellite data

Pieralberto Maianti · Marco Rusmini · Riccardo Tortini · Giorgio Dalla Via · Federico Frassy · Andrea Marchesi · Francesco Rota Nodari · Marco Gianinetto

Received: 26 February 2013 / Accepted: 7 February 2014 / Published online: 13 April 2014

P. Maianti (✉) · G. Dalla Via · F. Frassy · A. Marchesi · F. Rota Nodari · M. Gianinetto (✉)
Laboratory of Remote Sensing (L@RS), Department of Architecture, Built Environment and Construction Engineering (ABC), Politecnico di Milano, Via Ponzio 31, 20133 Milan, Italy
e-mail: pieralberto.maianti@polimi.it

M. Gianinetto
e-mail: marco.gianinetto@polimi.it

M. Rusmini
ERM Italia S.p.A., Via San Gregorio 38, 20124 Milan, Italy

R. Tortini
Department of Geological and Mining Engineering and Sciences, Michigan Technological University, 1400 Townsend Drive, Houghton, MI 49931-1295, USA

1 Introduction

Crude oil is a key asset for modern societies and usually several transfers have to be managed in order to get hydrocarbons from the oilfields to refineries, industries and then to the final customers. During these movements, oil spills may occur on land or water and, in the latter case, waves, wind and marine currents can spread large slicks in open water in a matter of hours (Fingas 2001). Depending on their extension and thickness, oil spills can generate considerable environmental and social impacts. In seawater, their main effect is to undermine the ecosystem through the poisoning of birds, aquatic organisms and phytoplankton in particular, which are at the base of the marine food chain and pass the absorbed hydrocarbons to all the upper trophic feeding levels (Graham et al. 2010). Furthermore, fishing and tourism industries of coastal regions can be compromised for years, generating economic losses on a large scale.

The quick detection and continuous tracking of oil slicks are key factors for monitoring the diffusion of pollutants in the environment, and satellite remote sensing is able to provide a synoptic coverage of the affected area in short time (Jha et al. 2008). Traditionally, synthetic aperture radar (SAR) has proven to be a useful technology for the mapping of oil slicks. For example, radar sensors are not constrained by cloud coverage and exhibit a higher sensitivity to oil slicks in comparison with optical imagery, but they have a longer revisit time and does not have capabilities neither for oil thickness estimation nor for oil type recognition (Brekke and Solberg 2005), and the semi-automatic detection of oil slicks is biased by look-alikes such as natural films/slicks, grease ice, threshold wind speed areas, wind sheltering by land, rain cells, shear zones, internal waves and other similar problems (Espedal 1999; Fiscella et al. 2000; Brekke and Solberg 2005). Nevertheless, medium-resolution satellite SAR systems are still among the most used for the detection of surface oil slicks because of their all-weather and day and night imaging capabilities.

In the past years, several authors evaluated the use of optical sensors for the mapping of oil slicks. Airborne sensors usually offer higher spatial and spectral resolution compared with satellite sensors, and the data acquisition is flexible enough to follow the quick dynamics of oil slicks (Wadsworth et al. 1992; Fingas and Brown 1997b; Lennon et al. 2006; Fingas and Brown 2011). Unfortunately, these imaging systems are expensive and not suitable for the mapping of large areas. On the other hand, the long revisit time of medium-resolution sun-synchronous optical satellites and the coarse spatial resolution of short revisit time geostationary and polar-orbiting optical satellites have limited the use of such technology in the past (Shi et al. 2007; Casciello et al. 2007). In addition, both airborne and satellite optical sensors need cloud-free sky and good atmospheric conditions, further decreasing the chances to appropriately map the evolution of oil slicks (Espedal and Johannessen 2000). An emblematic case is the Exxon Valdez oil spill (1989), where a slick covered large parts of the Gulf of Alaska for more than a month, but only a single cloud-free optical image was available due to unfortunate weather conditions (Noerager and Goodman 1991).

Nevertheless, the number of operational civilian optical satellites currently in orbit around the Earth is greater than that of SAR and is increasing constantly; hence, optical data for a specific region are usually available with considerable shorter revisit times. Hu et al. (2003) demonstrated the possibility of monitoring large oil slicks using the Moderate-Resolution Imaging Spectroradiometer (MODIS) sensor onboard NASA's Terra and Aqua satellites, and its capability of operational use has been confirmed by other more recent studies (Shi et al. 2007; Li et al. 2009; Leifer et al. 2012). However, the surface oil slick

detection with optical data is a complex task due to a sensible dependence on various variables, like the physical oil characteristics, sea surface roughness, weather and illumination conditions (Jha et al. 2008; Fingas and Brown 1997a).

Due to the aforementioned issues, up to now, no standard data processing technique has been presented to detect oil slicks with optical images. This paper describes a new method for the tracking of surface oil slicks using MODIS imagery, which is based on the fluorescence/emissivity index (Gianinetto et al. 2010a) and object-based image analysis OBIA (Rusmini et al. 2012). Two case studies are presented: the Deepwater Horizon (DWH) and the Campos Basin (CB) oil spill accidents.

2 Case studies

The first case study is the Deepwater Horizon oil spill (2010), which represents the largest documented accidental marine oil spill in history (Leifer et al. 2012). A dramatic explosion occurred on April 20, 2010 (Fig. 1), causing the collapse of the submarine drilling rig on the British Petroleum (BP) operated Macondo prospect, about 80 km off the Louisiana coast (USA). The spill came from a broken pipe leaking at about 1.5 km under the sea surface and reached a total estimated amount of 4.9 million barrels (NOAA 2010) until the flow was stopped in July 2010 (BP 2010). During the first 8 days, the oil quickly expanded on the sea surface and covered a vast area, spanning almost 120 km from North to South. In the same few days, the slick reached the Delta National Wildlife Refuge and the Breton National Wildlife Refuge, which constitute the main parts of Mississippi river delta ecosystem (Martin et al. 2002).

The second case study is the marine oil spill occurred during November 2011 in the deep waters of the Campos Basin production field (Fig. 2), about 140 km southeast from the Brazilian coastline. Here, an underestimation of the pressure at an oil reservoir explored by Chevron caused hydrocarbon leakage for about 8 days, with the spreading of a large amount of oil on the seawater (Energy-pedia 2012).

3 Methods

3.1 Dataset

Moderate-Resolution Imaging Spectroradiometer is a 36-band multispectral sensor with a multi-resolution cell size ranging from 250 m to 1,000 m, onboard the EOS AM (Terra) and EOS PM (Aqua) satellites. The satellites' orbits are timed so that Terra crosses the descending node at about 10:30 a.m. local time and Aqua crosses the ascending node at about 1:30 p.m. local time, with a maximum potential revisit time of 2 days.

All the MODIS L1B data have been made available through the NASA Level 1 and Atmosphere Archive and Distribution System (LAADS) website (http://ladsweb.nascom.nasa.gov).

On the DWH study area, 70 MODIS scenes imaged both from Terra and Aqua between April 20, 2010, and July 14, 2010, were acquired and evaluated. Among them, a time series composed of 12 daytime multispectral images was selected for being appropriately cloud-free and particularly relevant for the study (Table 1). The availability of two additional TIR data imaged nighttime has been considered as well in order to broaden the dataset.

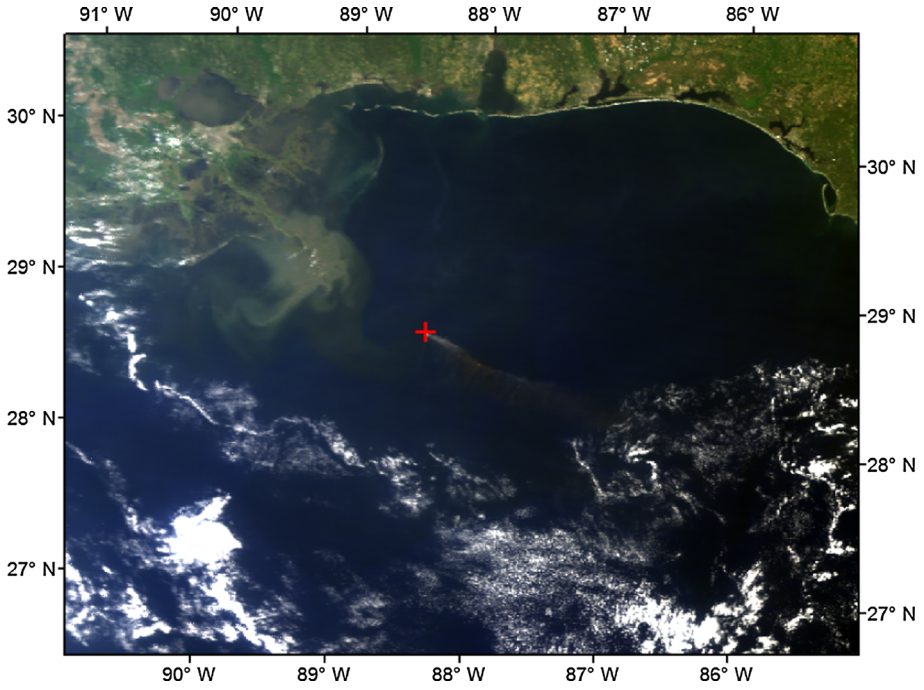

Fig. 1 Deepwater Horizon oil spill. Terra-MODIS image of the study area collected on April 21, 2010. The red cross shows the location of the drilling rig explosion with the smoke plume flowing from the platform on fire

On the CB study area, 13 MODIS scenes imaged both from Terra and Aqua between November 4, 2011, and November 25, 2011, were acquired and evaluated. Among them, only 3 daytime multispectral images were selected for analysis (Table 2). Unfortunately, no additional TIR nighttime images were suitable to broaden the CB dataset.

Only for the DWH blowout were reference data available, courtesy of the US National Oceanic and Atmospheric Administration (NOAA), as a set of vector shape files of the oil slick's perimeter throughout the satellites' passages, with the exclusion of the days April 27 and May 4 and 5. These data were generated by the NOAA National Environmental Satellite, Data and Information Service (NESDIS), which manually integrated numerous imagery sources, including SAR and high-resolution visible imagery, along with various ancillary data sources during the entirety of the crisis time period (www.ssd.noaa.gov/PS/MPS/deepwater.html). NOAA shape files were used as ground truth for the validation of the results.

The CB accident was very small in comparison with the DWH disaster and may be considered as one of the many oil spills that occur each year and go unnoticed. Although no official reference data have been reported for this event, it resulted in remarkable damage to marine ecosystems (Oceana 2011; Ocean Power Magazine.net 2011).

3.2 Theoretical background

The remote sensing technology always has been considered useful in damage assessment and relief operations for mapping surface oil extension (Al-Hinai et al. 1993; Bentz and de

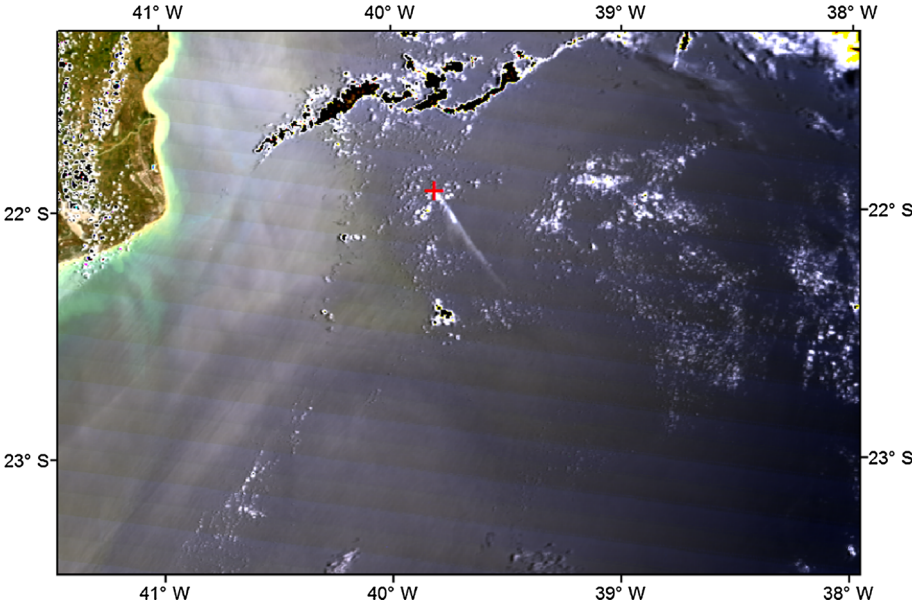

Fig. 2 Campos Basin oil spill. Terra-MODIS image of the study area collected on November 9, 2011. The red cross shows the location of Campos Basin production field

Table 1 Deepwater Horizon case study. MODIS time series used

Date	Time (local)	Satellite
April 21, 2010	11:05	Terra
April 25, 2010	13:55	Aqua
April 27, 2010	13:40	Aqua
April 29, 2010	02:30	Terra
April 29, 2010	11:55	Terra
May 4, 2010	13:50	Aqua
May 5, 2010	23:10	Aqua
May 9, 2010	14:05	Aqua
May 11, 2010	13:55	Aqua
May 17, 2010	11:40	Terra
June 9, 2010	11:50	Terra
June 26, 2010	11:45	Terra
July 12, 2010	14:05	Aqua
July 14, 2010	13:55	Aqua

Miranda 2001; Dessì et al. 2008; Hu et al. 2003; Jha et al. 2008), oil thickness and oil type (Fingas et al. 1998; Goodman 1989). Therefore, oil spectral properties have been extensively studied in past.

Oil seems to have no specific spectral features in the visible that can be used for a straightforward detection (Jha et al. 2008). However, in some special circumstance, oil slick may appear silvery with a higher reflectance than the background. Furthermore, some

Table 2 Campos Basin case study. MODIS time series used

Date	Time (local)	Satellite
November 9, 2011	11:05	Terra
November 11, 2011	10:55	Terra
November 12, 2011	14:20	Aqua

specific sun-surface-sensor geometries may lead to signal saturation (sunglint) regardless of the surface, being it water or oil (Fingas and Brown 1997a).

In the near-infrared, oil has some weak spectral features near 1.00 and 1.20 μm (Lammoglia and Filho 2011), although they appear to be of little utility for an operational detection from satellite. At longer wavelengths, hydrocarbon exhibits specific absorption features in the short-wave infrared (Gianinetto et al. 2010b) such as the aromatic absorptions near 1.67 and 2.15 μm or the alkane absorptions near 1.73 and 2.30 μm (Clark et al. 2010). Nevertheless, depending on their spectral setup, broadband satellites imaging systems may not be suitable for their detection, while airborne hyperspectral sensors could.

On the other hand, oil is characterized by a strong ultraviolet fluorescence, (Salisbury et al. 1993; Brivio et al. 2006; Clark et al. 2010), but these wavelengths typically are not recorded with optical sensors (both airborne or satellite) due to low atmospheric transmittance in this spectral window.

Moreover, oil is optically thick, and therefore, absorbs the solar radiation and re-emits part of it in the thermal infrared region (TIR, 8–14 μm) (Clark et al. 2009; Lammoglia and Filho 2011). Consequently, in the TIR, thick oil slicks appear sensibly brighter than water, whereas thinner slicks still appear sufficiently brighter and flimsy slicks are not detectable (Jha et al. 2008).

Salisbury et al. (1993) demonstrated that the spectral behavior of seawater and oil slicks in the TIR is well distinguishable and practically unaffected by environmental variables. Hence, one unambiguous distinction mark between the two surfaces is the lower emissivity of oil compared to water.

At nighttime the spectral signature of oil is characterized by a lower emissivity than water. Jha et al. (2008) reported that during the daytime, thick oil absorbs greater amounts of radiation and, as a result, it appears hotter than water. At nighttime, the reverse behavior is observed: heat loss in oil is faster than in water and, therefore, thick oil appears cooler than water. Hover and Plource (1994) reported that the TIR sensors RS-18C and WF-360TL nighttime images were able to detect oil and water with high contrast from different flight altitudes. However, differences in the kinetic temperature of seawater and oil may induce the detection of false targets. In summary (Salisbury et al. 1993):

- Oil features change from daytime to nighttime;
- Water surface roughness, as well as sea foam, influences the slick's spectral properties because the waves oriented at a specular angle backscatter the sunglint;
- Despite the lower emissivity of oil compared to water in the TIR, the variability of water's real kinetic temperature may induce false positives and biases in the detection of oil slick.

Based on these assumptions, the fluorescence/emissivity index (FEI) has been designed specifically to take into account for a higher reflectance of oil in the blue wavelength (induced by both fluorescence or reflected light) and a lower emissivity in the TIR region (Eq. 1):

$$FEI = \frac{\rho_{\text{Blue}} - \varepsilon_{\text{Thermal}}}{\rho_{\text{Blue}} + \varepsilon_{\text{Thermal}}} \quad (1)$$

where ρ_{Blue} is the reflectance calculated for the MODIS spectral band nr.3 (0.459–0.479 μm); $\varepsilon_{\text{Thermal}}$ is the emissivity calculated for the MODIS spectral band nr.31 (10.780–11.280 μm).The FEI is a normalized index ranging from −1 to +1 and higher values correspond to surfaces characterized by the typical features of oil spectra described above (Gianinetto et al. 2010a).

3.3 Data processing

The DWH dataset was geo-referenced in UTM-WGS84 17 N and clipped between 30°36′30″ N 91′19′47″ W and 26°43′39″ N 85°1′3″ W, while the CB dataset was geo-referenced in UTM-WGS84 24S and clipped between 21°15′55.81″ S 41°25′56.98″ W and 23°28′13.34″ S 37°57′31.58″ W.

After the geocoding, the image segmentation was applied to the two time series using the highest spatial resolution data (MODIS bands nr.1 and nr.2) and the following parameters:

- Scale factor = 300;
- Shape = 0.1;
- Compactness = 0.5;

The *scale factor* is a parameter that determines the maximum heterogeneity allowed in the segments and, therefore, controls the size of the objects (Frauman and Wolff 2005), while *shape* and *compactness* are parameters that control the outline and the dependency of objects to spectral and geometrical features (Maxwell 2010). Figure 3 shows the differences between the image segmentation performed on 250 m and 1,000 m spatial resolution data.

Next, each image object has been classified with a k-Nearest Neighbors rule (kNN) using as input data the reflectance values of MODIS spectral bands nr.1 (0.620–0.672 μm), nr.3 (0.459–0.479 μm) and nr.4 (0.545–0.565 μm), with the addition of the FEI index computed at object level. This multi-resolution approach made possible to put together data with different geometric resolution (250, 500 and 1,000 m) in a single classification environment.

Unfortunately, no ground reference was available as training data; thus, four classes (i.e., clouds, shallow water, deep water and oil) have been defined and recognized on the images. The additional class "land" was defined using the shoreline of the ancillary vector data provided by courtesy of NOAA. For each class, some training samples were selected depending on the scene content (Tables 3, 4). On the additional, nighttime MODIS images available for the DWH case study, both image segmentation and classification were carried on using the spectral band nr.32 (11.770–12.270 μm) because of its high noise-equivalent temperature difference. Table 5 shows the number of the selected training samples.

A further post-classification was applied to the class "oil", generating the class "oil slick" based on the following rules:

- Oil slick is an homogeneous surface composed of one or more "oil" objects;
- The single objects composing the oil slick must be contiguous or at most separated by just one intermediate non-oil segment;
- The oil slick is defined as the largest group of objects with the properties mentioned above.

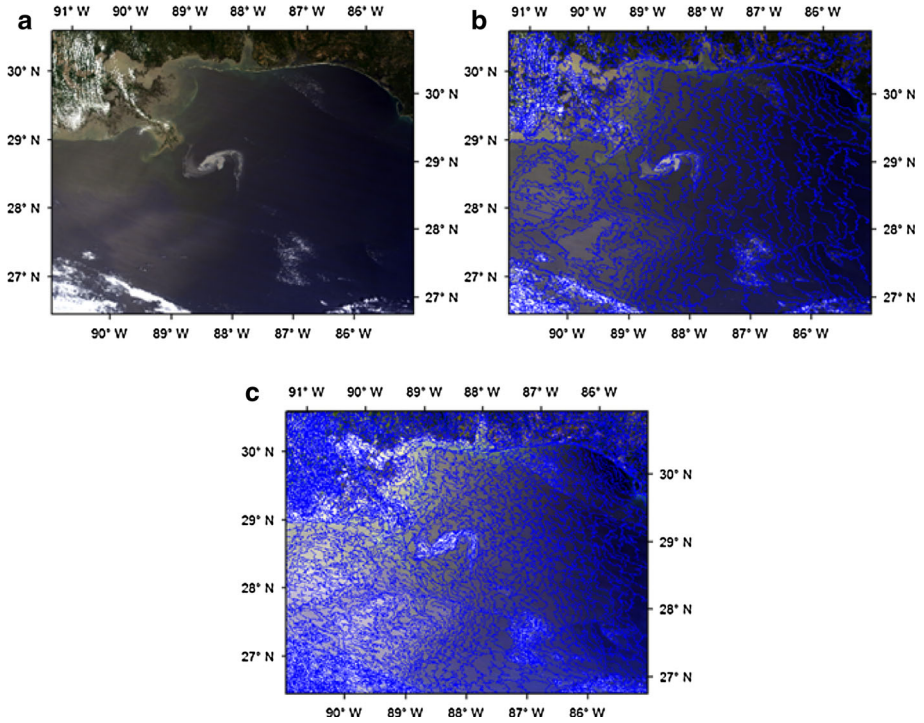

Fig. 3 Deepwater Horizon case study. **a** Terra-MODIS image of the study area collected on April 29, 2010; **b** example of image segmentation on 1,000 m spatial resolution data; **c** example of image segmentation on 250 m spatial resolution data

Consequently, some objects initially classified as "oil" were rejected and those retained were re-labeled as "oil slick." Similarly, the classes "shallow water" and "deep water" were both merged in the class "water". Figure 4 exemplifies the effect of the post-classification.

4 Results

Classification maps produced with the OBIA (Fig. 5) show how the size of the oil slicks is highly variable during the emergency time period. The shape and the extension show extremely fast dynamics due to currents, wind, oil leakage flux variability and human mitigation actions. Table 6 summarizes the estimated area of the oil slicks and their distance from the coastline, estimated measuring the minimum distance between the coastline and the border of the recognized oil slicks.

Although the volume of oil discharged in the early days of the emergency was significant, limited satellite observations were possible until mid-May, when the surface slick increased of almost five times in just 6 days (i.e., from May 11 to May 17) and reached its maximum extension on June 9. Figure 6 describes some of the surface oil slick's shape changes during the survey: For each date, an ellipse is used to describe the extension (area), the principal direction (major axes) and the centroid (barycenter) of the surface oil slick.

Table 3 Training samples (objects) collected on the Deepwater Horizon daytime dataset

Date	Time (local)	Number of training samples per class			
		Clouds	Shallow water	Deep water	Oil
April 21, 2010	11:05	8	5	15	0
April 25, 2010	13:55	10	4	9	3
April 27, 2010	13:40	4	8	15	3
April 29, 2010	11:55	8	4	12	4
May 4, 2010	13:50	5	7	13	1
May 9, 2010	14:05	2	14	9	8
May 11, 2010	13:55	8	3	9	6
May 17, 2010	11:40	5	8	23	14
June 9, 2010	11:50	13	5	20	22
June 26, 2010	11:45	14	2	3	15
July 12, 2010	14:05	11	5	31	6
July 14, 2010	13:55	3	4	19	5

Table 4 Training samples (objects) collected on the Campos Basin dataset

Date	Time (local)	Number of training samples per class			
		Clouds	Shallow water	Deep water	Oil
November 9, 2011	11:05	4	9	23	3
November 11, 2011	10:55	9	11	27	3
November 12, 2011	14:20	3	8	37	18

Table 5 Additional training samples (objects) collected on the Deepwater Horizon nighttime dataset

Date	Time (local)	Number of training samples per class			
		Clouds	Shallow water	Deep water	Oil
April 29, 2010	02:30	5	2	4	1
May 5, 2010	23:10	6	2	10	1

The minor and major axes of the ellipses lay on the directions of minimum and maximum area extension and represent 1/8 of the standard deviation values of the spatial distribution.

Similar to the DWH case study, classification maps generated for the CB dataset are characterized by a large variability in the shape and extension of the surface oil slick during the accident. Figures 7 and 8 show the mapping and the changes over time of the slick, while the estimated areas are summarized in Table 7.

5 Discussion

The DWH emergency can be divided into three different phases on the base of the oil slick surface retrieved from the MODIS time series (Fig. 9):

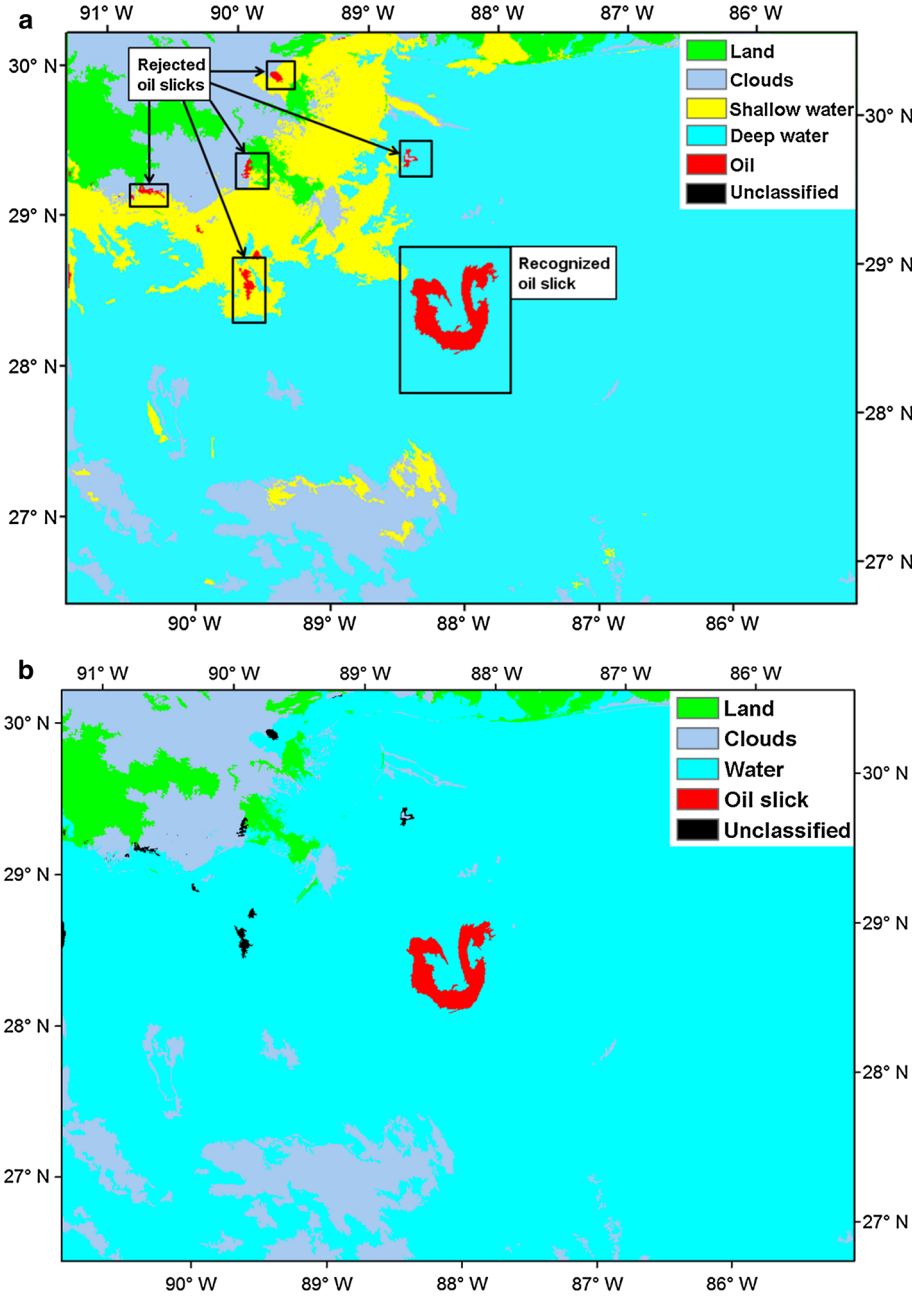

Fig. 4 Deepwater Horizon case study. **a** Identification of the oil on Aqua-MODIS imagery of May 9, 2010; **b** oil slick after post-classification

- First mapping of the oil slick (from April 25 to May 11);
- Rapid increase in the oil slick (from May 11 to June 26);
- Oil spill reduction and emergency conclusion (from June 26 to July 15).

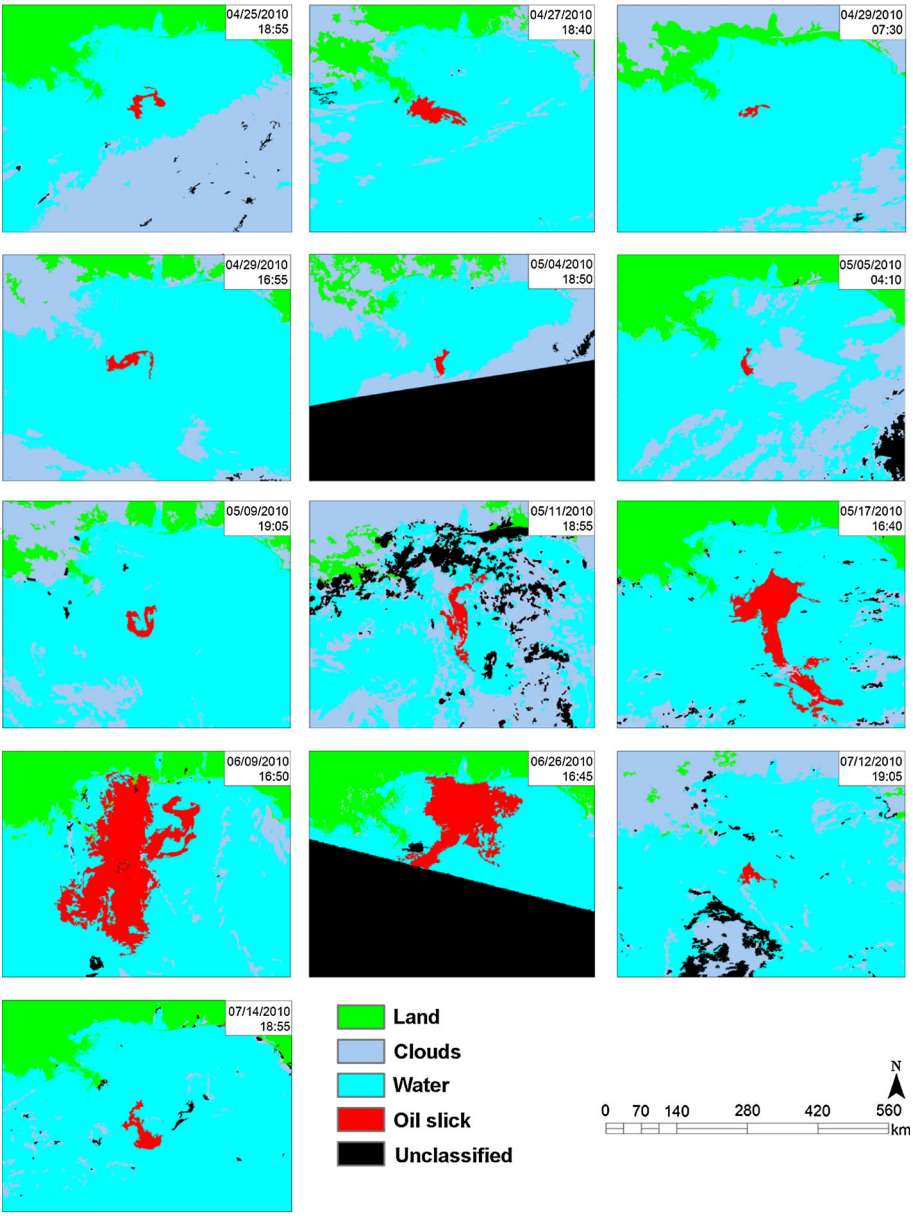

Fig. 5 Deepwater Horizon case study. Object-based classification maps

For each period, the estimated oil extent was compared with a detailed report of the events from the official federal portal for the Deepwater BP oil spill response and recovery (www.restorethegulf.gov) and the online edition of the New Orleans local journal - The Times-Picayune (www.nola.com). In detail:

Table 6 Deepwater Horizon case study. Estimated area of the oil slick during the emergency period

Date	Time (local)	Estimated area (km^2)	Distance oil slick-coast (km)
April 25, 2010	13:55	1,383	54.9
April 27, 2010	13:40	3,185	12.4
April 29, 2010	02:30	590	18.8
April 29, 2010	11:55	1,714	55.5
May 4, 2010	13:50	734	59.9
May 5, 2010	23:10	644	55.1
May 9, 2010	14:05	1,838	65.9
May 11, 2010	13:55	3,696	76.0
May 17, 2010	11:40	15,924	26.2
June 9, 2010	11:50	43,917	0.0
June 26, 2010	11:45	21,784	0.0
July 12, 2010	14:05	1,084	72.7
July 14, 2010	13:55	491	81.5

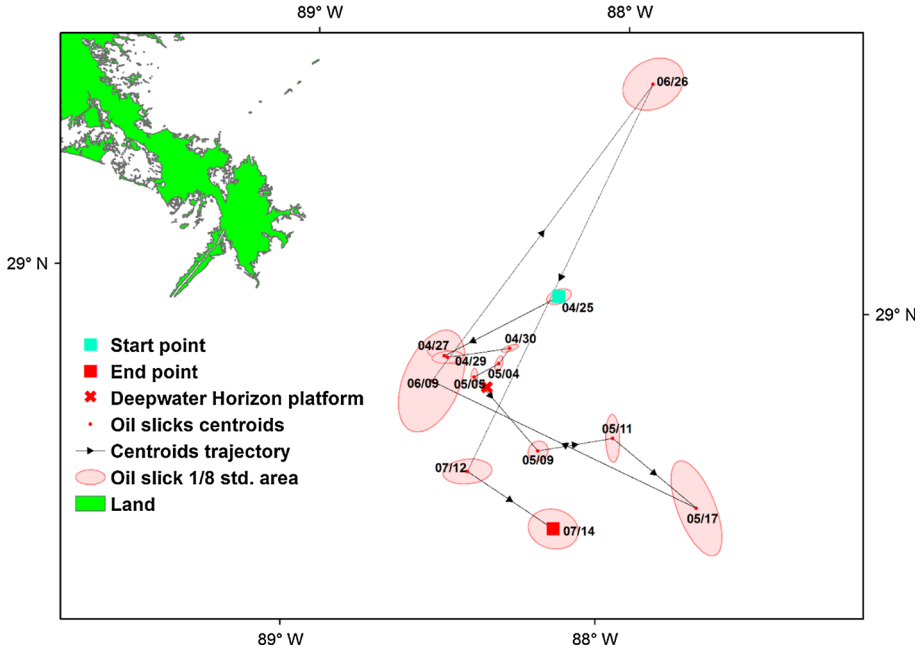

Fig. 6 Deepwater Horizon case study. The ellipses represent the surface oil slick's shape features (area, principal directions and barycenter) variation during the survey

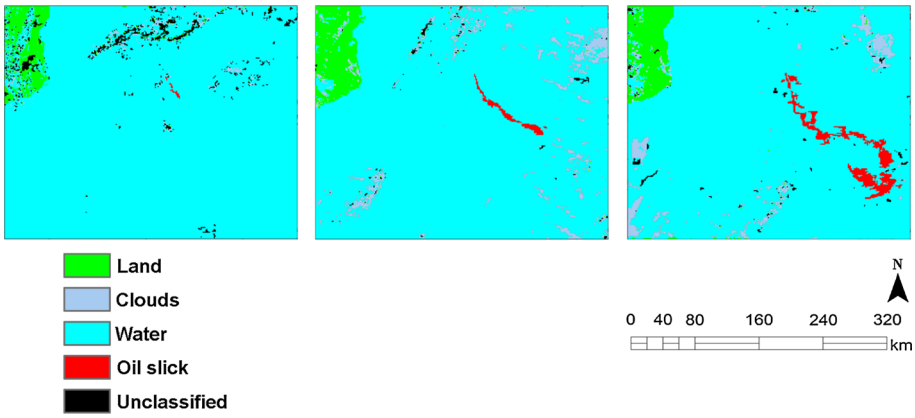

Fig. 7 Campos Basin case study. Object-based classification maps

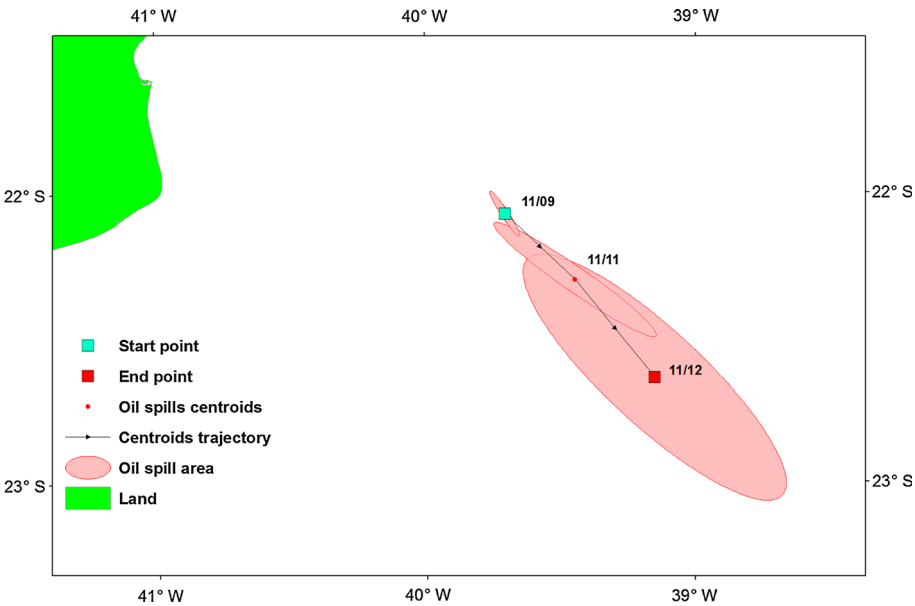

Fig. 8 Campos Basin case study. The ellipses represent the surface oil slick's shape features (area, principal directions and barycenter) variation during the survey

Table 7 Campos Basin case study. Estimated area of the oil slick

Date	Time (local)	Estimated area (km^2)	Distance oil slick-coast (km)
November 9, 2011	11:05	83	122.8
November 11, 2011	10:55	734	119.0
November 12, 2011	14:20	3,635	108.3

Phase 1

- May 5, 2010: One leak is capped but the flow does not diminish;
- May 9, 2010: Frozen hydrates log the box, the effort fails;

Phase 2

- May 19, 2010: First signs of thick oil found near the mouth of Mississippi;
- May 25, 2010: "Top kill" operation starts;
- May 29, 2010: "Top kill" operation fails;
- June 4, 2010: "Cut and cap" operation captures some oil on the ocean surface;
- June 16, 2010: A second containment system siphons more oil;
- June 24, 2010: The cap system works again;

Phase 3

- July 3, 2010: Oil skimmer restarts working again after the passage of hurricane Alex;
- July 12, 2010: New containment cap is placed on the gushing well;
- July 15, 2010: The new capping stack stops oil flow for the first time since April;
- July 19, 2010: Completion of the relief well by BP.

The oil slick mapped from satellite coherently matched the order of events reported by The Times-Picayune and the federal portal for the Deepwater BP oil spill response and recovery (Fig. 9). After the accident and the first spill, the inability to seal effectively the leakage and to contain the oil in a bounded area led to a rapid increase in the slick. The passage of hurricane Alex in the Gulf of Mexico had a remarkable impact on the operations related to the spill's containment and cleanup, when in addition the oil skimmers failed. However, the wind-induced drift caused by the northward winds played an important role in limiting both the spread of surface oil inside the Gulf of Mexico and in entering the Loop Current (Le Henaff et al. 2012). Finally, a sequence of successful interventions on the leaking well led first to a reduction, and successively to the complete extinction of the oil flux placing a capping stack on the well.

The accuracy evaluation of the class "oil slick" was performed comparing the surface slicks mapped with MODIS with the slick's perimeter provided by courtesy of NOAA and used as reference data, when available (Fig. 10). Table 8 and Table 9 show, respectively, the comparison of data and the accuracy assessment.

It should be noted that the reference data of April 29 was associated with the daytime MODIS image (11:15 local time) rather than the nighttime image (02:30 local time), which then was excluded from the accuracy assessment.

Results show that the extension of the surface oil slick as retrieved from satellite data always is underestimated compared with the NOAA reference vector files, except for June 9, where it is overestimated.

The major source of error is due to cloud cover. On one hand, clouds may obscure most of the oil slick; on the other hand, sheen may be misclassified with clouds, leading to an overall underestimation of the surface slick. These issues affected the classification of the MODIS images recorded on May 11, June 9, June 26 and July 12.

Another source of error is related to the geometric resolution of MODIS. Being a moderate spatial resolution sensor, the detection of small or sparse patches of oil is less effective and accurate than using higher resolution or airborne sensors, as it was for the generation of the reference data. This limitation is clearly noticeable in the classification of MODIS images acquired by the sensor on April 29, May 9, July 12 and July 14. Here, the

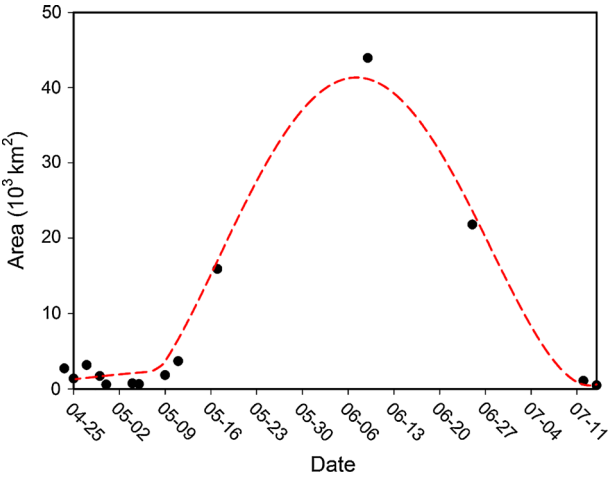

Fig. 9 Deepwater Horizon case study. Variation in the oil slick area (dots) observed with MODIS, and a polynomial interpolation (dashed line) of the represented area values

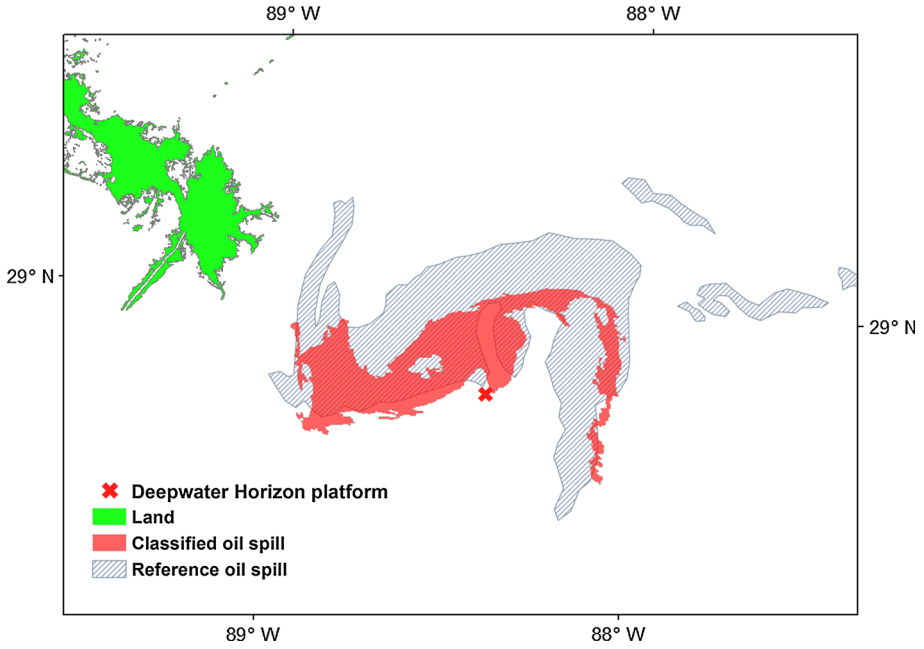

Fig. 10 Deepwater Horizon case study. Example of comparison (April 29, 2010) between the NOAA reference data and the classified oil slick

mapped oil slick is underestimated because the finer shapes of the slicks are not recorded by MODIS, despite no significant cloud cover is present nearby the slick.

False positives may be produced also by other marine sources of thermal anomalies, such as Langmuir rows. These shallow and slow wind-aligned roll vortices at the Ocean's

Table 8 Deepwater Horizon case study. Mapped oil slicks compared to the reference data

Date	Oil slick area (km^2)				
	Classified (satellite)	Reference (NOAA)	Intersection	Commission	Omission
April 25, 2010	1,383	1,483	1,090	292	392
April 27, 2010	Unavailable reference data				
April 29, 2010	1,714	4,091	1,580	134	2,511
May 4, 2010	Unavailable reference data				
May 5, 2010	Unavailable reference data				
May 9, 2010	1,838	3,876	1,732	106	2,144
May 11, 2010	3,697	8,477	3,250	447	5,227
May 17, 2010	15,925	24,477	12,027	3,898	7,022
June 9, 2010	43,918	24,045	16,912	27,006	7,134
June 26, 2010	21,785	32,420	14,609	7,175	17,810
July 12, 2010	1,316	4,062	1,148	167	2,914
July 14, 2010	3,414	6,469	2,886	528	5,022

Table 9 Deepwater Horizon case study. Accuracy assessment

Date	Time (local)	Producer accuracy (%)	User accuracy (%)	Commission error (%)	Omission error (%)
April 25, 2010	13:55	73.5	78.9	21.1	26.5
April 27, 2010	13:40	Unavailable reference data			
April 29, 2010	11:55	38.6	92.2	7.8	61.4
May 4, 2010	13:50	Unavailable reference data			
May 5, 2010	23:10	Unavailable reference data			
May 9, 2010	14:05	44.7	94.2	5.7	55.3
May 11, 2010	13:55	38.3	87.9	12.1	61.7
May 17, 2010	11:40	49.1	75.5	24.5	28.7
June 9, 2010	11:50	70.3	38.5	61.5	29.7
June 26, 2010	11:45	45.1	67.1	32.9	54.9
July 12, 2010	14:05	28.3	87.3	12.7	71.7
July 14, 2010	13:55	44.6	84.5	15.5	77.6

surface can strongly facilitate transport processes (Kukulka et al. 2012) and tend to accumulate organic material in surface, including the macroalga Sargassum which has non-zero spectral reflectance at 400 nm and is visible in satellite imagery (Zhong et al. 2012). Further research is necessary to address these specific phenomena here not considered.

The source of errors mentioned above can have an impact not only on the calculation of the slick's surface but also on the representation of its changes over time. Figures 6 and 8 show the use of ellipses to represent the main slick's features: area, principal direction (major axis) and location (centroid). More in depth, results show that the overall under-estimation of the surface slick, namely shape and area, may be responsible for an incorrect estimation of its trajectory, evaluated as the movement of its centroid (Fig. 11).

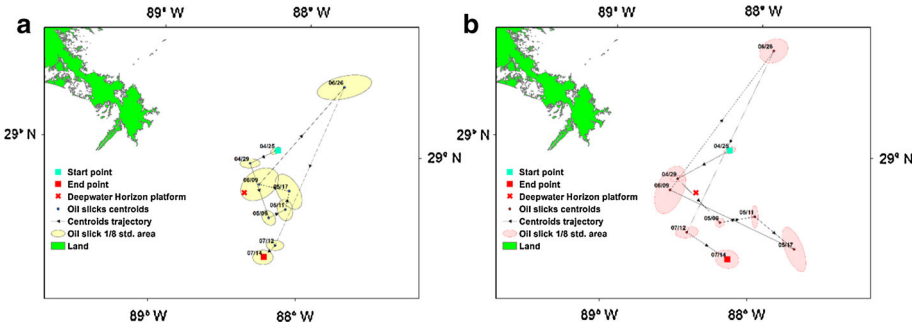

Fig. 11 Deepwater Horizon case study. Qualitative comparison between the ellipses representing the reference (**a**) and the mapped (**b**) surface oil slick changes during the survey

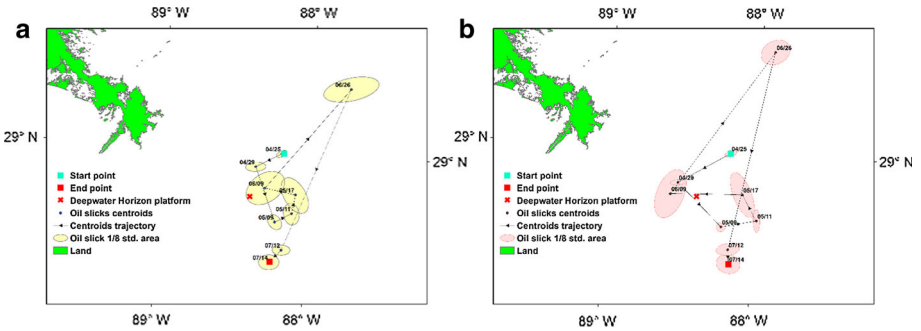

Fig. 12 Deepwater Horizon case study. Qualitative comparison between the ellipses representing the reference (**a**) and the mapped (**b**) surface oil slick changes during the survey, after removing the gross error in the centroids' position for the dates of June 17 and July 14

Table 10 Deepwater Horizon case study. Evaluation of the slick's orientation

Date	Estimated slick's orientation	Reference slick's orientation
April 25, 2010	E	NE
April 29, 2010	E	E
May 9, 2010	NE	SE
May 11, 2010	S	S
May 17, 2010	SE	SE
June 9, 2010	N	NE
June 26, 2010	NE	E
July 12, 2010	E	E
July 14, 2010	E	E

As it can be seen in Fig. 12, after removing the gross error in the centroids' position for the dates of June 17 and July 14, both due to an underestimation of the western slick's surface, the trajectory of the surface slick estimated with MODIS accurately approximates

the reference coordinates provided by NOAA. Regarding the orientation of the slicks, determined by the direction of the ellipse's major axis, those mapped with MODIS are reasonably similar to that calculated from the NOAA reference data, with the exclusion of the date of May 9 (Table 10).

Although no reference data have been released for the CB leakage, this case study proved that MODIS data are suitable as well for the monitoring of smaller and short duration oil spills (Table 7; Fig. 8).

6 Conclusions

This study demonstrates how moderate resolution optical satellite images can be used for monitoring large offshore oil spills. The fluorescence/emissivity index here discussed exploits the theoretically higher reflectance of oil at shorter wavelengths and the lower emissivity in the thermal infrared region, combined with object-based image analysis, for the mapping of oil slicks. Results obtained for the Deepwater Horizon event are in accordance with the list of containment efforts reported by the local press and are correlated with the ground truth provided by the US National Oceanic and Atmospheric Administration. On the other hand, the Campos Basin case study shows how smaller short duration oil spills can be detected and monitored as well, although no reference data were available for validation.

The main advantages of the proposed method are its straightforward implementation, fast semi-automatic data processing capability, near real-time data availability and availability of both daytime and nighttime images. Furthermore, cloud-cover permitting, MODIS has a near daily potential revisit time. However, a limit of this study was the impossibility to evaluate the oil mapping at night because no ground truth was available for comparison.

The results of this study suggest that satellite moderate resolution optical data can be included in an operational monitoring system for oil slicks. The main field of application of images collected with MODIS and similar sensors should be multi-source data assimilation (e.g., with SAR data) and integration with standard monitoring methods and models.

Acknowledgments The authors are grateful to NASA for making available MODIS L1B data through LAADS. The authors would like also to thank NOAA National Environmental Satellite, Data and Information Service (NESDIS) and in particular Jennifer Belge for providing the reference data utilized in this study.

References

Al-Hinai KG, Khan MA, Dabbagh AE, Bader TA (1993) Analysis of Landsat Thematic Mapper data for mapping oil slick concentrations—Arabian Gulf oil spill 1991. Arab J Sci Eng 18(2):85–93

Bentz C, de Miranda FP (2001) Application of remote sensing data for oil spill monitoring in the Guanabara Bay. Proc IGARSS01 Rio de Janeiro Brazil 1:333–335. doi:10.1109/IGARSS.2001.976149

Brekke C, Solberg AHS (2005) Oil spill detection by satellite remote sensing. Remote Sens Environ 95(1):1–13. doi:10.1016/j.rse.2004.11.015

British Petroleum (2010) Gulf of Mexico restoration—containing the leak. http://www.bp.com/sectiongenericarticle800.do?categoryId=9036583&contentId=7067603

Brivio PA, Lechi G, Zilioli E (2006) Principi e metodi di Telerilevamento. Città Studi—De Agostini, Milano

Casciello D, Lacavat T, Pergolat N, Tramutoli V (2007) Robust satellite techniques (RST) for oil spill detection and monitoring. Proceedings of 4th international workshop on the analysis of multitemporal remote sens images pp 1–6. doi:10.1109/MULTITEMP.2007.4293040

Clark RN, Curchin JM, Hoefen TM, Swayze GA (2009) Reflectance spectroscopy of organic compounds: 1. Alkanes. J Geophys Res Planets 114(E3):E03001. doi:10.1029/2008JE003150
Clark RN, Swayze GA, Leifer I, Livo KE, Kokaly R, Hoefen T, Lundeen S, Eastwood M, Green RO, Pearson N, Sarture C, McCubbin I, Roberts D, Bradley E, Steele D, Ryan T, Dominguez R, the Air borne Visible/Infrared Imaging Spectrometer (AVIRIS) Team (2010) A method for quantitative mapping of thick oil spills using imaging spectroscopy. U.S. Geol Surv Open-File Report 2010–1167
Dessì F, Melis MT, Naitza L, Marini A (2008) MODIS data processing for coastal and marine environment monitoring: a study on anomaly detection and evolution in Gulf of Cagliari (Sardinia, Italy). Int Arch Photogramm Remote Sens Spat Inf Sci XXXVII(B8), Beijing (China):695–698
Espedal HA (1999) Satellite SAR oil spill detection using wind history information. Int J Remote Sens 20(1):49–65. doi:10.1080/014311699213596
Espedal HA, Johannessen OM (2000) Detection of oil spills near offshore installation using synthetic aperture radar. Int J Remote Sens 21(11):2141–2144. doi:10.1080/01431160050029468
Energy-pedia news 27 Feb 2012 (2012) Brazil: Statoil announces new Brazilian pre-salt oil discovery in Campos Basin Block BM-C-33. http://www.energy-pedia.com/news/brazil/new-149305
Fingas M (2001) The basics of oil spill cleanup. CRC Press LLC, Boca Raton (Florida)
Fingas MF, Brown CE (1997a) Remote sensing of oil spills. Sea Technol 38:37–46
Fingas MF, Brown CE (1997b) Review of oil spill remote sensing. Spill Sci Technol Bull 4:199–208. doi:10.1016/S1353-2561(98)00023-1
Fingas MF, Brown CE (2011) Oil spill remote sensing: a review. Oil Spill Sci Technol 6:111–147
Fingas MF, Brown CE, Mullin JV (1998) The visibility limits of oil on water and remote sensing thickness detection limits. Proceeding of the fifth thematic conference on remote sensing for mar and coast environ, environmental research institute of Michigan, Ann Arbor (Michigan), pp 411–418
Fiscella B, Giancaspro A, Nirchio F, Pavese P, Trivero P (2000) Oil spill detection using marine SAR images. Int J Remote Sens 21(18):3561–3566. doi:10.1080/014311600750037589
Frauman E, Wolff E (2005) Segmentation of very high spatial resolution satellite images in urban areas for segments-based classification. Int Arch Photogramm Remote Sens Spat Inf Sci, Tempe (AZ), USA XXXVI part 8/W27:1-4
Gianinetto M, Maianti P, Tortini R, Rota Nodari F, Lechi G (2010a) Evaluation of MODIS data for mapping oil slicks—the Deepwater Horizon oil spill case. In: Calado H, Gil A (eds) Geogr Technol applied to Mar Spat Plan and Integr Coast Zone Manag. Universidade Dos Açores
Gianinetto M, Rota Nodari F, Maianti P, Tortini R, Lechi G (2010b) Multispectral technology for mining exploration in arid lands: a short review. Italian J Remote Sens 42(2):3–12. doi:10.5721/ItJRS20104221
Goodman RH (1989) Application of the technology in North America. The remote sensing of oil slicks. Wiley, Chichester, pp 39–65
Graham WM, Condon RH, Carmichael RH, D'Ambra I, Patterson HK, Linn LJ, Hernandez FJ Jr (2010) Oil carbon entered the coastal planktonic food web during the Deepwater Horizon oil spill. Environ Res Lett 5(045301):1–6. doi:10.1088/1748-9326/5/4/045301
Hover GL, Plource JV (1994) Evaluation of night capable sensors for the detection of oil on water. U.S. Dep of Transportation, rep No. CG-D-09-94
Hu C, Muller-Karger FE, Taylor CJ, Myhre D, Murch B, Odriozola AL, Godoy G (2003) MODIS detects oil spills in Lake Maracaibo, Venezuela. EOS Trans Am Geophys Union 84(33):313–319. doi:10.1029/2003EO330002
Jha MN, Levy J, Gao Y (2008) Advances in remote sensing for oil spill disaster management: state-of-the-art sensors technology for oil spill surveillance. Sensors 8:236–255. doi:10.3390/s8010236
Kukulka T, Plueddemann AJ, Sullivan PP (2012) Nonlocal transport due to Langmuir circulation in a coastal ocean. J Geophys Res Oceans 117(C12007):1–17. doi:10.1029/2012JC008340
Lammoglia T, Filho CRdS (2011) Spectroscopic characterization of oils yielded from Brazilian offshore basins: potential applications of remote sensing. Remote Sens Environ 115(10):2525–2535. doi:10.1016/j.rse.2011.04.038
Le Henaff M, Kourafalou VH, Paris CB, Helgers J, Aman ZM, Hogan PJ, Srinivasan A (2012) Surface evolution of the Deepwater Horizon oil spill patch: combined effects of circulation and wind-induced drift. Environ Sci Technol 46:7267–7273. doi:10.1021/es301570w
Leifer I, Lehr WJ, Simecek-Beatty D, Bradley E, Clark R, Dennison P, Hu Y, Matheson S, Jones CE, Holt B, Reif M, Roberts DA, Svejkovsky J, Swayze G, Wozencraft J (2012) State of the art satellite and airborne marine oil spill remote sensing: application to the BP Deepwater Horizon oil spill. Remote Sens Environ 124:185–209. doi:10.1016/j.rse.2012.03.024
Lennon M, Babichenko S, Thomas N, Mariette V, Mercier G, Lisin A (2006) Detection and mapping of oil slicks in the sea by combined use of hyperspectral imagery and laser-induced fluorescence. Proc EARSeL 5(1/2006):120–128

Li Y, Lan G, Li J, Ma L (2009) Potential analysis of maritime oil spill monitoring based on MODIS thermal infrared data. Proceedings of 2009 IEEE international geoscience and remote sensing symposium, vol 3, pp 373–376. doi:10.1109/IGARSS.2009.5417780

Martin JF, Reyes E, Kemp GP, Mashriqui H, Day JW Jr (2002) Landscape modeling of the Mississippi delta. Bioscience 52(4):357–365. doi:10.1641/0006-3568(2002)052[0357:LMOTMD]2.0.CO;2

Maxwell SK (2010) Generating land cover boundaries from remotely sensed data using object-based image analysis: overview and epidemiological application. Spat Spatio-Temporal Epidemiol 1:231–237. doi:10.1016/j.sste.2010.09.005

NOAA (2010) Federal science report details fate of oil from BP spill. http://www.noaanews.noaa.gov/stories2010/20100804_oil.html

Noerager JA, Goodman RH (1991) Oil tracking, containment and recovery during the EXXON VALDEZ response. Proceedings of 1991 oil spill conference, American Petroleum Institute, Washington DC, pp 193–203. doi:10.7901/2169-3358-1991-1-193

Ocean Power Magazine.net (2011) Major oil spill in Brazil's campos basin caused by Chevron's deepwater drilling. http://www.oceanpowermagazine.net/2011/11/21/major-oil-spill-in-brazil%E2%80%99s-campos-basin-caused-by-chevrons-deepwater-drilling

Oceana (2011) Major oil spill in Brazil's campos basin caused by deepwater drilling. http://oceana.org/en/news-media/press-center/press-releases/major-oil-spill-in-brazil-s-campos-basin-caused-by-deepwater-drilling

Rusmini M, Candiani G, Frassy F, Maianti P, Marchesi A, Rota Nodari F, Dini L, Gianinetto M (2012) High-resolution SAR and high-resolution optical data integration for sub-urban land-cover classification. 2012 IEEE international geoscience and remote sensing symposium (IGARSS 2012), Munich, Germany, pp 4986–4989. doi:10.1109/IGARSS.2012.6352492

Salisbury JW, D'Aria DM, Sabins FF Jr (1993) Thermal infrared remote sensing of crude oil slicks. Remote Sens Environ 45(2):225–231. doi:10.1016/0034-4257(93)90044-X

Shi L, Zhang X, Seielstad G, Zhao C, He MX (2007) Oil spill detection by MODIS images using fuzzy cluster and texture feature extraction. Proceedings of OCEANS 2007-Europe, pp 1–5. doi:10.1109/OCEANSE.2007.4302485

Wadsworth A, Looyen WJ, Reuter R, Petit M (1992) Aircraft experiments with visible and infrared sensors. Int J Remote Sens 13(6–7):1175–1199. doi:10.1080/01431169208904186

Zhong Y, Bracco A, Villareal TA (2012) Pattern formation at the ocean surface: sargassum distribution and the role of the eddy field. Limnol Oceanogr Fluids Environ 2:12–27. doi:10.1215/21573689-1573372